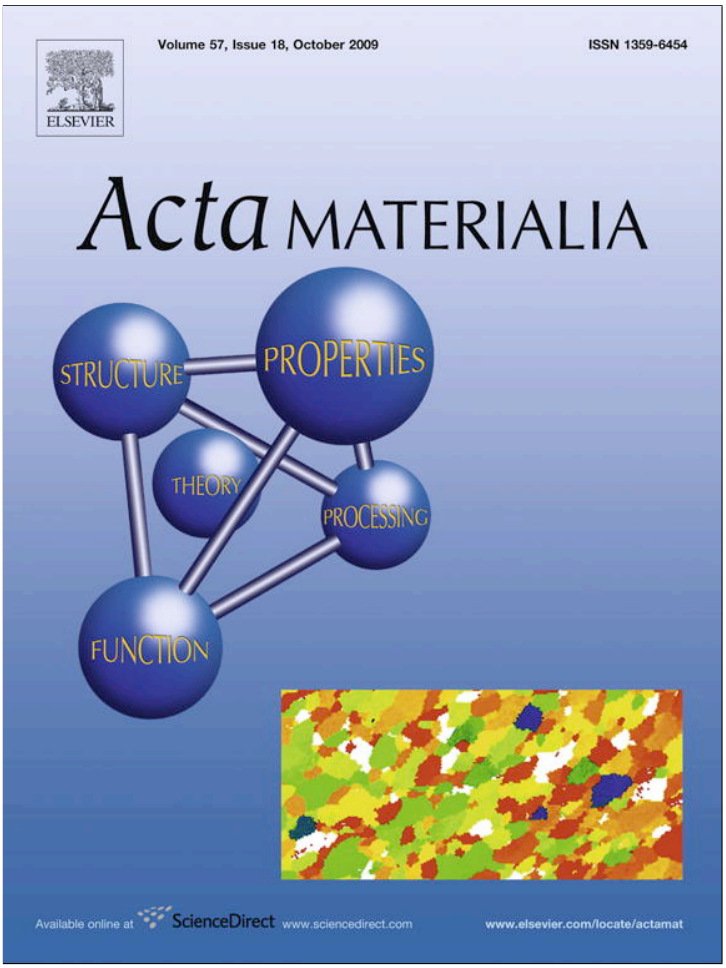

Available online at www.sciencedirect.com
ScienceDirect
Acta Materialia 57 (2009) 5531–5542
Acta MATERIALIA
www.elsevier.com/locate/actamat

A molecular dynamics study of self-diffusion in the cores of screw and edge dislocations in aluminum

G.P. Purja Pun, Y. Mishin *

Department of Physics and Astronomy, George Mason University, MSN 3F3, 4400 University Drive, Fairfax, VA 22030-4444, USA

Received 1 June 2009; received in revised form 24 July 2009; accepted 26 July 2009
Available online 21 August 2009

Abstract

Self-diffusion along screw and edge dislocations in Al is studied by molecular dynamics simulations. Three types of simulations are performed: with pre-existing vacancies in the dislocation core, with pre-existing interstitials, and without any pre-existing defects (intrinsic diffusion). We find that diffusion along the screw dislocation is dominated by the intrinsic mechanism, whereas diffusion along the edge dislocation is dominated by the vacancy mechanism. Diffusion along the screw dislocation is found to be significantly faster than diffusion along the edge dislocation, and both diffusivities are in reasonable agreement with experimental data. The intrinsic diffusion mechanism can be associated with the formation of dynamic Frenkel pairs, possibly activated by thermal jogs and/or kinks. The simulations show that at high temperatures the dislocation core becomes an effective source/sink of point defects and the effect of pre-existing defects on the core diffusivity diminishes.

Keywords: Dislocation; Diffusion; Vacancy; Interstitial; Computer simulation

1. Introduction

The mobility of atoms in core regions of lattice dislocations can be orders of magnitude higher than in surrounding lattice regions. For historic reasons, this phenomenon is often referred to as "pipe diffusion", although it should properly be called "dislocation diffusion" for consistency with the well-established terms of grain boundary diffusion and surface diffusion [1–3].

The fast atomic transport along dislocations can play a significant role in the kinetics of many processes in materials [4]. Dislocation diffusion can contribute to creep mechanisms, including dislocation climb and Orowan loop bowing [5]. Deviations from the power law of creep can be attributed to dislocation diffusion [6,7]. Diffusion of solute atoms along arrested dislocations is one of the proposed mechanisms of dynamics strain aging in alloys exhibiting flow instabilities [8–10]. The kinetics of solute segregation to surfaces and grain boundaries can be enhanced by diffusion along dislocations terminating at the interfaces [11–13]. Coarsening kinetics in precipitation-strengthened alloys are often influenced or even controlled by dislocation diffusion, especially in nanometer-scale structures in which dislocation lines can directly connect the growing particles. Diffusion along misfit dislocations at γ/γ' interfaces can contribute to the γ'-phase coarsening and rafting kinetics, affecting the creep resistance of superalloys [14]. Dislocation diffusion can influence sintering processes [15–17], oxidation, corrosion, recovery of radiation damage, and electromigration damage in microelectronic devices [18].

Despite its importance, the phenomenon of dislocation diffusion is not well understood on the fundamental level. The amount of reliable experimental information is rather limited [1–3]. According to experimental data available, the coefficient D_d of dislocation diffusion approximately follows the Arrhenius law

$$D_d = D_d^0 \exp\left(-\frac{E_d}{k_B T}\right), \tag{1}$$

* Corresponding author. Tel.: +1 703 993 3984; fax: +1 703 993 1993.
E-mail address: ymishin@gmu.edu (Y. Mishin).

1359-6454/$36.00
doi:10.1016/j.actamat.2009.07.048

k_B being the Boltzmann constant and T temperature. The activation energy of dislocation diffusion, E_d, is approximately 0.6–0.7 of the activation energy of lattice diffusion E, whereas the pre-exponential factor D_d^0 is close to typical values for lattice diffusion [1]. Dislocation diffusion coefficients tend to increase with the magnitude of the Burgers vector and decrease with the dissociation width into Shockley partials in face-centered cubic metals. It is assumed that dislocation diffusion is mediated by atomic exchanges with single vacancies, although there is no convincing experimental evidence for this mechanism. In fact, except for the analogy with lattice diffusion, there is no fundamental reason why vacancy diffusion must necessarily dominate over interstitial diffusion or other possible diffusion mechanisms.

Experimental measurements of dislocation diffusion are difficult and can be divided in two categories. In *direct* measurements, the diffusion coefficient is extracted from the penetration profile (concentration vs. depth) of radioactive tracer or impurity atoms diffused into a deformed single crystal or a polycrystal containing low-angle grain boundaries. The penetration profile is analyzed in terms of continuum models, in which the dislocations are represented by high-diffusivity "pipes" of some radius r_d whose diffusion coefficient D_d is much larger than the lattice diffusivity D. Several mathematical solutions of this diffusion problem have been developed [3], all assuming that the dislocations are normal to the surface and arranged in a wall or another (e.g., hexagonal) periodic array. By fitting a model solution to the experimental profile, the so-called integrated diffusion flux $P_d = D_d A_d$ is extracted, where $A_d = \pi r_d^2$ is the cross-sectional area of the dislocation "pipe". To estimate D_d separately, an assumption about r_d must be made, which is usually $r_d = 0.5$ nm. This uncertainty of r_d does not affect applications since it is only the quantity P_d that appears in all models of diffusion-controlled processes in materials, not D_d separately. Most of the dislocation diffusion coefficients available today were measured in the 1960–1970s. Very few direct measurements are made these days, see [19] (radiotracer self-diffusion in Fe) and [20,21] (secondary-ion mass spectrometry for oxides) as some recent examples.

In *indirect* methods, P_d is back-calculated from the rate of a particular diffusion-controlled process, such as internal friction, dislocation climb, dislocation loop shrinkage, phase growth kinetics [22,18], or annihilation of dislocation dipoles [1,23,21]. Essentially, it can be any process whose rate is assumed to be controlled by dislocation diffusion and for which a model containing P_d is available. Unfortunately, such models often rely on crude approximations and contain other unknown parameters. Indirect measurements are only accurate up to an order of magnitude at best and have a poor reproducibility.

As one example relevant to this work, Table 1 summarizes experimental data for Al self-diffusion. For dislocation diffusion, only indirect measurements from void-shrinkage kinetics are available [24]. For dislocation diffusion in Al alloys, only crude estimates of the activation energy from internal friction experiments [25] exist in the literature.

The enhanced atomic mobility along dislocations and the correlation $E_d \approx 0.6 - 0.7E$ were confirmed by early atomistic simulations with pair potentials [26–28]. Contrary to the common assumption, Huang et al. [27,28] found that vacancies and interstitials could make comparable contributions to dislocation diffusion. More accurate simulations employing embedded-atom method (EAM) potentials have recently been performed for dislocations in Au [29], Al [30–33,4] and Cu [27–29], as well as Al–Mg [33] and Al–Cu [34] alloys. The rates of vacancy jumps along the core were found to depend on the dislocation character (edge, screw or mixed). However, except for [4,29], only diffusion by the vacancy mechanism was analyzed. Furthermore, while the diffusion coefficient of vacancies, D_v, was calculated in several studies [28–31], the atomic diffusion coefficient D_d was only estimated in Refs.

Table 1
Summary of experimental data for the pre-exponential factor D_0 and activation energy E of lattice diffusion, grain-boundary diffusion, and dislocation diffusion in Al. δ is the grain boundary width and A_d is the cross-sectional area of the dislocation core. The dash indicates that data is unavailable.

	Lattice diffusion		Boundary diffusion		Dislocation diffusion	
	D_0 (m^2/s)	E (eV)	δD_{0b} (m^3/s)	E_b (eV)	$A_d D_{0d}$ (m^4/s)	E_d (eV)
Lundy and Murdock [51]	1.71×10^{-4}	1.47	–	–	–	–
Volin et al. [24]	–	–	–	–	7.0×10^{-25}	0.85
Engardt and Barnes [52]	–	1.3	–	–	–	–
Spokas and Slichter [53]	–	1.40	–	–	–	–
DeSorbo and Turnbull [54]	–	1.44	–	–	–	–
Fradin and Rowland [55]	3.5×10^{-6}	1.25	–	–	–	–
Stoebe and Dawson [56]	0.02×10^{-4}	1.22	–	–	–	–
Stoebe and Dawson [56]	1.7×10^{-4}	1.48	–	–	–	–
Häßner [57]	–	–	1.9×10^{-14}[a]	0.62	–	–
Gangulee and d́Heurle [58]	–	–	2.3×10^{-22}	–	–	–
Levenson [59]	–	–	–	0.55	–	–
Haruyama et al. [60]	–	–	–	–	–	0.90
Federighi [61]	–	1.33	–	–	–	–
Volin and Balluffi [62]	1.76×10^{-5}	1.31	–	–	–	–

[a] 1.9×10^{-5} m^2/s multiplied by $\delta = 1.0$ nm.

[28,33,34] and determined by direct simulations only in Ref. [4]. We emphasize that it is D_d, not the point-defect diffusion coefficient, that controls the mass flux along the dislocation core and appears in all models of diffusion-controlled processes. The point-defect diffusion coefficient constitutes only one ingredient of the diffusion process, which must be combined with point-defect concentrations, jump-correlation factors and other ingredients to obtain D_d [35]. For impurity diffusion, the equilibrium segregation and impurity-defect binding energies at different sites should also be known [10,34].

An alternative and more straightforward approach adopted in [4] is to extract D_d from mean-squared atomic displacements computed by *direct* molecular dynamics (MD) simulations. An additional advantage of this approach is that information about diffusion mechanisms can be *inferred* from MD results, instead of postulating particular mechanisms as it is done in other methods. Recent simulation studies of grain boundary diffusion [36–41] have revealed a large variety of possible diffusion mechanisms, some of which cannot operate in the lattice. A similar multiplicity and complexity of diffusion mechanism might exist in dislocation cores.

The goal of this paper is to study the effect of the dislocation character on diffusion, and to evaluate the relative importance of vacancies and interstitials. We analyze the limiting cases of the edge and screw dislocations in Al, applying MD simulations to extract the diffusion coefficients in both dislocations. To make this paper self-contained, we include some of our earlier preliminary results for the screw dislocation [4].

2. Methodology

The atomic interactions are modeled with the EAM potential for Al developed in [42]. This potential is accurately fit to experimental and *ab initio* data and reproduces a number of properties of Al, including elastic constants, phonon frequencies, the intrinsic stacking fault energy, and point-defect formation and migration energies. The melting temperature T_m of Al predicted by this potential is 1042 K [43], which is about 10% above the experimental value. The predicted activation energy of bulk diffusion in Al is 1.33 eV [42] in good agreement with experiment [44,45].

A cylindrical model is used with a periodic boundary condition along the cylinder axis z. For the screw dislocation, the z axis is parallel to the crystallographic direction $[1\,1\,0]$, whereas the x and y axes are aligned with $[\bar{1}\,1\,2]$ and $[\bar{1}\,1\,1]$, respectively. The length of the cylinder is 47 Å and its initial diameter is about 150 Å. To create a dislocation, all atoms are displaced from their initially perfect lattice positions according to the anisotropic linear elasticity solution for a straight screw dislocation [46] with the Burgers vector $\frac{1}{2}[1\,1\,0]$. The elastic center is placed between atomic rows so that to avoid the singularity. After the displacements, a smaller cylinder is cut out of the large one, containing only 7344 atoms and having the same length but a smaller diameter of 58 Å. Atoms within a 6 Å thick outer layer of this smaller cylinder are fixed and all other atoms are relaxed by minimizing the total potential energy with respect to atomic positions. The relaxed structure of the dislocation core is found to be slightly dissociated into Shockley partials on a $\{1\,1\,1\}$ plane. This dissociation is very narrow but can be readily resolved by the Nye tensor method (see Fig. 3 in [47]) or other visualization techniques [48]. For a diffusion study, more atoms of this relaxed configuration are fixed, leaving only $N = 2064$ atoms free to move during the subsequent MD simulations. These free atoms are located within a cylinder of $d = 30$ Å in diameter centered at a midpoint between the partials. The goal of this step is to create a model with a relatively small number of dynamic atoms that would permit long MD runs.

A similar procedure has been applied to create an edge dislocation. In this case, the cylinder axis z is parallel to $[1\,1\,2]$, whereas the x and y directions are aligned with $[1\,\bar{1}\,0]$ and $[1\,1\,\bar{1}]$, respectively. The cylinder has the diameter and length of 100 Å and 50 Å, respectively, and contains 23,450 atoms. The Burgers vector $\frac{1}{2}[1\,1\,0]$ of the edge dislocation is parallel to x and the splitting of the partials is slightly larger than for the screw dislocation. For diffusion simulations, only $N = 4570$ atoms are left free to move, while all other atoms are fixed. The free atoms are located within a cylinder of $d = 44$ Å in diameter.

Dislocation diffusion has been studied at several temperatures from 750 K to 1000 K, the highest temperature being 42 K below the melting point with this potential. The MD simulations employ the ITAP Molecular Dynamics (IMD) code [49], with the integration time step of 2 fs. The NVT ensemble is implemented, with the temperature controlled by a Nose–Hoover thermostat. To minimize thermal stresses that might arise at high temperatures, the simulation block is expanded uniformly by the thermal expansion factor at the chosen temperature prior to the MD simulations. The thermal expansion factors predicted by this potential were computed earlier [43]. In each MD run, the temperature is ramped up to the target value during the first 2 ns, followed by isothermal annealing for at least 30 ns.

At the post-processing stage, the isothermal anneal time is divided into several equal intervals from 3 to 7 ns each, depending on the temperature. For each time interval, we identify all dynamic atoms located within an imaginary cylinder of a chosen radius $R < d/2$ in the beginning and at the end of the time interval. The mean-squared displacement $\langle z^2(t)\rangle$ of all such atoms parallel to the dislocation line is calculated as a function of time t. The functions $\langle z^2(t)\rangle$ computed for individual time intervals are then averaged over all intervals. This calculation is repeated for several values of R, producing a function $\langle z^2(t)\rangle(R)$ used for extracting the dislocation diffusion coefficients as will be discussed in Section 3.

Due to the periodic boundary condition in the z direction, an atom attempting to leave the block during the MD simulations is automatically translated back by the

repeat period of the block and reappears on its opposite side. By examining MD snapshots saved every 0.2 ns during the simulation run, all such translations across the block are identified and the atoms are moved back before using their coordinates for the calculation of $\langle z^2(t)\rangle$. We emphasize that this "unwrapping" procedure is implemented at the post-processing stage and by no means affects the actual MD simulations.

Three different types of simulations have been performed: when a single vacancy is created inside the dislocation core prior to the MD run, when a single self-interstitial is created, and when no point defects are introduced. The latter case will be referred to as *intrinsic* diffusion.

As will be discussed later, calculations of the diffusion coefficient after the introduction of a vacancy require the knowledge of the average number N_v of vacancies that would be found in the simulation block under equilibrium conditions at the given temperature. This number can be evaluated by

$$N_v = \sum_{n=1}^{N} \exp\left(-\frac{E_{vn}^f}{k_B T}\right), \tag{2}$$

where E_{vn}^f is the vacancy formation energy at site n, and the summation runs over all N positions of the dynamic atoms. The values of E_{vn}^f are obtained by separate calculations, in which a single vacancy is created at various sites and the block is relaxed statically at 0 K. From the energy difference ΔE_{vn} between the relaxed block with a vacancy and the initial relaxed block without a vacancy, E_{vn}^f is obtained by $E_{vn}^f = \Delta E_{vn} + E_0$, where $E_0 = -3.36$ eV is the equilibrium cohesive energy of the perfect crystal [42]. These calculations are simplified by the fact that the E_{vn}^f values in each atomic row running parallel to z are identical, therefore only one E_{vn}^f per row needs to be computed.

A similar procedure is applied to determine the equilibrium number N_i of interstitial atoms that would be found in the simulation block:

$$N_i = \sum_{n=1}^{K} \exp\left(-\frac{E_{in}^f}{k_B T}\right), \tag{3}$$

where the summation is over K stable interstitial configurations in and around the dislocation core region. The formation energy of bulk interstitials is so high that only a limited number of interstitial configurations in a narrow vicinity of the core make non-negligible contributions to Eq. (3). The interstitial formation energy is given by $E_{in}^f = \Delta E_{in} - E_0$, where ΔE_{in} is the total energy change due to the interstitial creation.

3. Results

3.1. Point defect energies in dislocation cores

For lattice vacancies, the EAM potential employed in this work gives the formation energy $E_v^f = 0.68$ eV and the migration energy $E_v^m = 0.65$ eV [42]. Thus, the activation energy of vacancy-mediated self-diffusion is predicted to be $E = E_v^f + E_v^m = 1.33$ eV. The lattice self-interstitial formation energy is much higher, 2.59 eV, even for the most stable ([0 0 1] split dumbbell) configuration.

The vacancy formation energies E_{vn}^f calculated for different sites n within the simulation block range from 0.51 eV to 0.71 eV for the screw dislocation and from 0.52 eV to 0.75 eV for the edge dislocation. The lowest values are found in the dislocation core region while the highest values near the boundary between the dynamic atoms and the fixed region (due to image forces). Our range of E_{vn}^f values is comparable to that computed by Hoagland et al. [30] using a different EAM potential. Fig. 1 displays contour

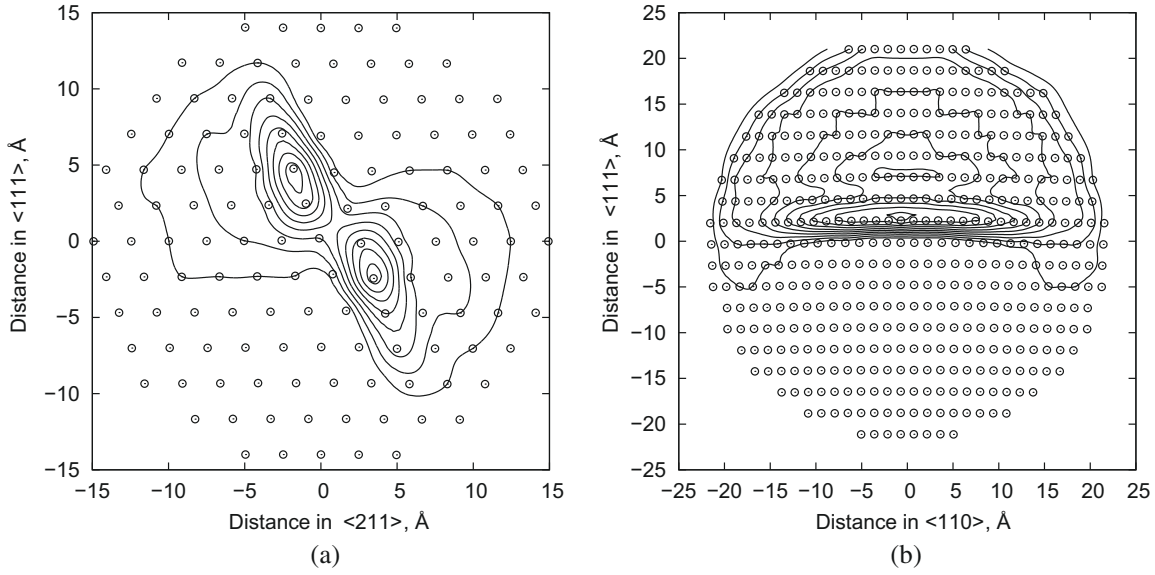

Fig. 1. Contour plots of the vacancy formation energy in the vicinity of (a) the screw dislocation and (b) the edge dislocation. The contour interval is 0.02 eV and the innermost contour corresponds to the energy of 0.52 eV. The bulk value of the vacancy formation energy is 0.68 eV. The dislocation line is normal to the page and the circles represent projections of the dynamic atoms.

plots of E^f_{vn} for both dislocations. For the screw dislocation, the contours clearly reveal the core splitting on the $(1\bar{1}1)$ plane, with minima of E^f_{vn} in the partial core regions (Fig. 1a). For the edge dislocation, the exact positions of the partials are not revealed by the contours but the splitting is clearly seen. The vacancy formation energy is reduced relative to its bulk value in the compression region above the glide plane (Fig. 1b).

The interstitial formation energy varies between 1.04 and 2.72 eV for the screw dislocation and between 0.89 and 2.84 eV for the edge dislocation. Again, the energies slightly exceeding the ideal bulk value (2.59 eV) are found near the fixed region. The lowest formation energies occur inside the dislocation core and rapidly increase to the bulk value at short distances away from the core.

3.2. Intrinsic diffusion along dislocation cores

An important finding of this work is the existence of the intrinsic diffusivity along the dislocation cores. Specifically, even without any pre-existing point defects, atoms are found to migrate along the screw dislocation core at all temperatures studied here and along the edge dislocation core at high temperatures. While intrinsic diffusion at high temperatures can be explained by the increasingly disordered core structure that becomes capable of generating point defects, the existence of intrinsic diffusion at low temperatures is an interesting and unexpected phenomenon. Before quantifying this effect, Fig. 2 gives its qualitative demonstration for the screw dislocation at 900 K. An arbitrary MD snapshot was taken, atoms located within a slice of material normal to the dislocation line were selected, and their motion was tracked through subsequent snapshots. The observed random scattering of the labeled atoms in both directions parallel to the dislocation line gives direct evidence of diffusive motion in the core region.

Typical time dependencies of mean-squared displacements of atoms are displayed in Fig. 3a. These plots were obtained for the screw dislocation with $R = 7$ Å, but they look qualitatively similar for the edge dislocation and for other values of R. It is seen that the plots accurately follow a linear relation expected from the Einstein formula $\langle z^2(t)\rangle = 2\bar{D}t$, confirming that our simulations have properly sampled the diffusion kinetics. The slope S of the least-squares linear fit to such plots gives the diffusion coefficient $\overline{D} = S/2$ averaged over the cylindrical region of the chosen radius R.

In the continuum models of dislocation diffusion (Section 1), the diffusion coefficient is assumed to be discontinuous and have a high value D_d inside a "pipe" of a radius r_d and a much smaller value outside the "pipe". In reality the diffusivity is continuous but can still be expected to have a sharp maximum in the core region. Accordingly, the diffusivity averaged over a cylindrical region of radius R, considered as a function of R, should also have a maximum in the core and fall off to zero at infinitely large R. The exact form of this function is unknown *a priori*, but after

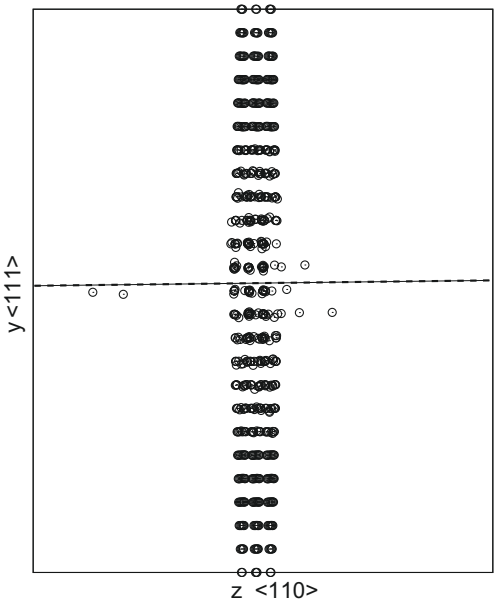

Fig. 2. Demonstration of atomic diffusion along the screw dislocation at 900 K in the absence of pre-existing point defects (intrinsic diffusion). The bounding box represents the dimensions of the cylindrical simulation block viewed from a side. The dislocation line is marked by a horizontal dashed line. Atoms initially located in a slice normal to the dislocation line were selected and their new positions after a 2 ns long MD run are shown in this plot. All other atoms remain invisible. The spreading of the selected atoms along the core is a signature of intrinsic diffusion.

trying several analytical forms we found that our simulation data is best described by a Gaussian function

$$\overline{D}(R) = Ae^{-R^2/r_d^2} + B, \tag{4}$$

with adjustable parameters A, B and r_d. Examples of fit with this equation are given in Fig. 4a. The absence of data points below a certain value of R is explained by limited statistics collected when the probing cylinder contains too few atoms. In addition, at small R the results begin to depend on the exact placement of the axis of the probing cylinder.

Parameter r_d in Eq. (4) has the obvious meaning of the dislocation core radius. Accordingly, $D^I_d \equiv \overline{D}(R = r_d) = A/e + B$ can be taken as an effective dislocation diffusivity. The superscript I is a reminder that this diffusivity is intrinsic. While in an infinitely large system B would be zero, in a finite-size system it is small but finite due to the effect of boundary conditions. To a good approximation, D^I_d can be evaluated as simply $D^I_d \approx A/e$.

The intrinsic diffusivities obtained for the screw dislocation approximately follow the Arrhenius law (1) (Fig. 5a) with the activation energy and pre-exponential factor given in Table 2. For the edge dislocation, we were able to determine the intrinsic diffusion coefficients only at temperatures 925 K and higher (Fig. 5b). They were found to be more than an order of magnitude smaller than for the screw dislocation. At lower temperatures, the intrinsic diffusivity of the edge dislocation is below the detection capabilities of our method and was not calculated. Comparison of these

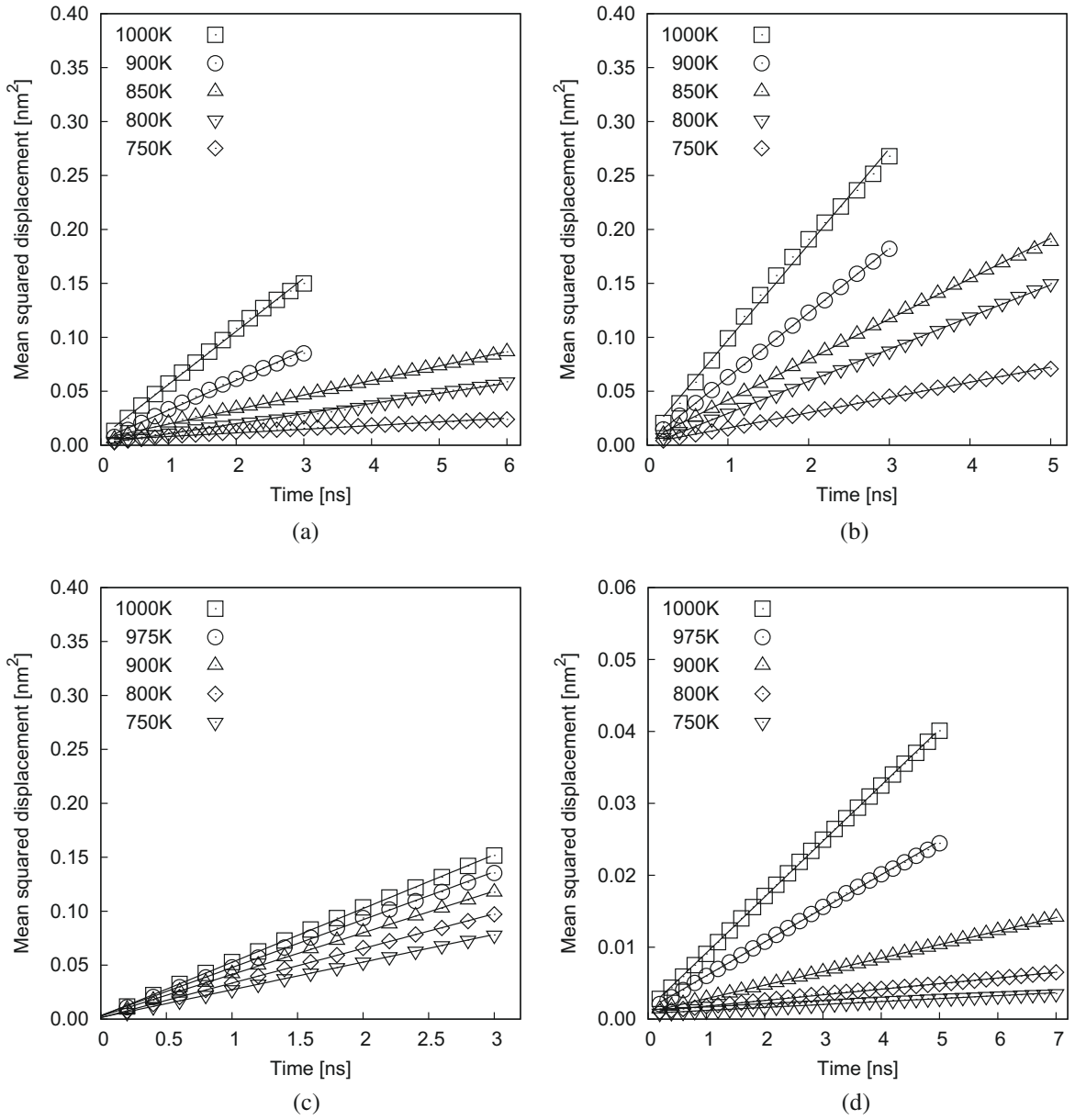

Fig. 3. Mean-squared atomic displacements along the core of the screw (a and b) and edge (c and d) dislocations as functions of time at selected temperatures: (a) in the absence of point defects (intrinsic diffusion), (b and d) in the presence of a single vacancy, (c) in the presence of a single interstitial. The displacements are averaged over a cylinder of radius $R = 7$ Å in (a–c) and 8 Å in (d).

results with diffusion by other mechanisms and with experimental data will be discussed later (Section 4).

3.3. Vacancy diffusion in dislocation cores

When a single vacancy is introduced into the dislocation core prior to the MD simulations, the plots of $\langle z^2(t)\rangle$ vs. t remain linear but their slopes increase relative to the intrinsic case (Fig. 3b and d), indicating an enhancement of diffusion by the vacancy. The average core diffusivity $\overline{D}(R)$ can again be fitted by Eq. (4), where parameter B represents the vacancy-mediated bulk diffusivity distorted by the boundary conditions (Fig. 4b and d). As in the intrinsic case, the quantity $D_d^{\mathrm{raw}} = A/e + B$ can be taken as the effective dislocation core diffusivity. However, this "raw" value needs to be corrected for the equilibrium vacancy concentration.

Indeed, in the MD simulations, the dynamic region of the simulation block contains exactly one vacancy at all temperatures. This single vacancy spends most of its time in the core (where it diffuses fast along the z direction) and a small fraction of the time in surrounding lattice regions (where it diffuses relatively slowly). The fixed boundaries prevent the vacancy from escaping and it remains confined to the dynamic region. Under real equilibrium conditions, however, the dynamic region would contain on average N_v vacancies, where N_v is given by Eq. (2). This number depends on temperature and, at most

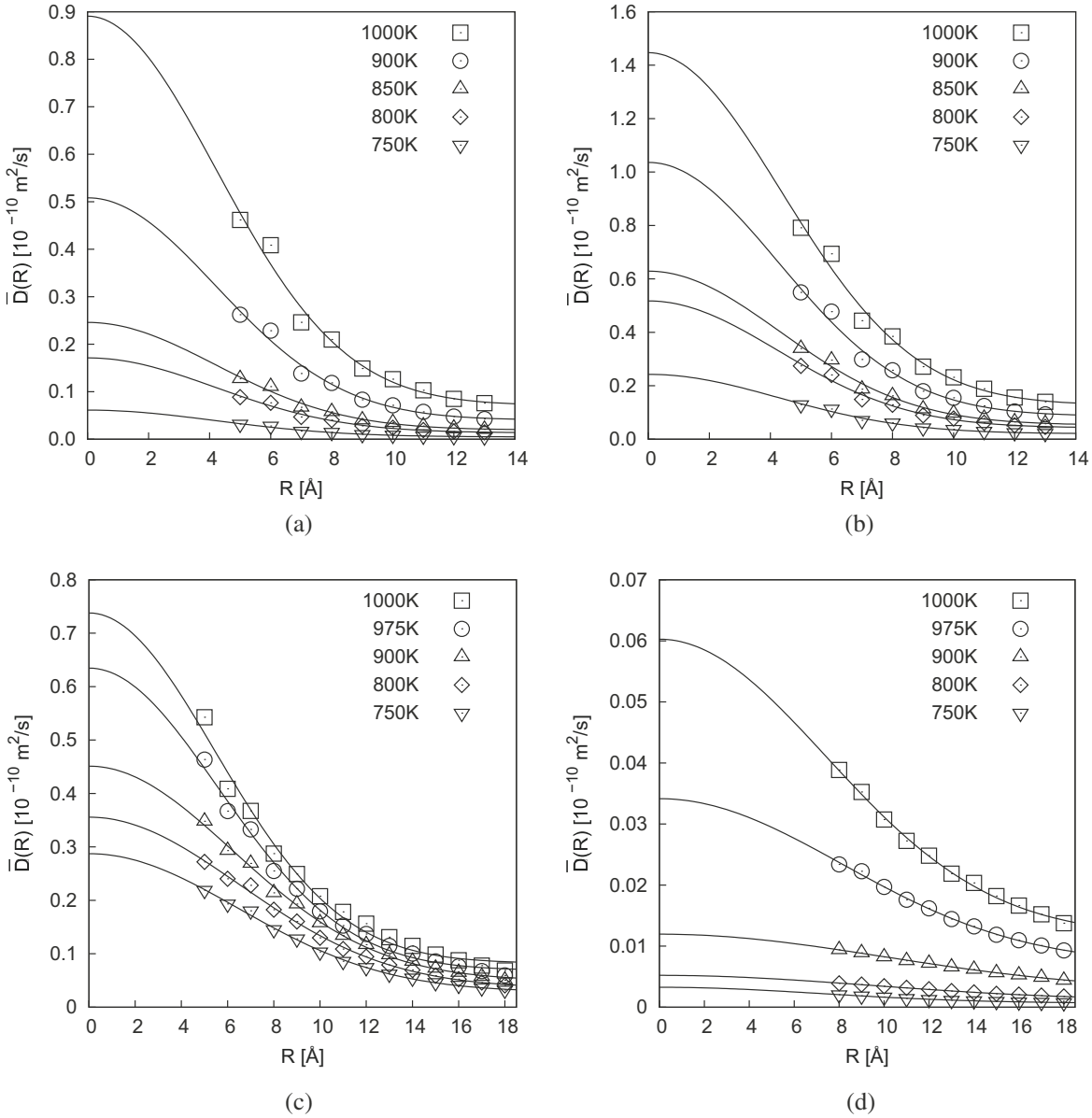

Fig. 4. Average dislocation diffusivity vs. radius R for the screw (a and b) and edge (c and d) dislocations as a function of time at selected temperatures: (a) in the absence of point defects (intrinsic diffusion), (b and d) in the presence of a single vacancy, (c) in the presence of a single interstitial. The lines present fits by Eq. (4).

temperatures studied here, remains smaller than one. Thus, the "raw" value D_d^{raw} overestimates the actual vacancy contribution to the dislocation diffusivity by a factor of $1/N_v$. Assuming that the intrinsic diffusion mechanism continues to operate in the presence of the vacancy, it can also contribute to D_d^{raw}. Thus, the true dislocation diffusivity D_d^v in the presence of equilibrium vacancies can be calculated by

$$D_d^v = D_d^I + N_v\left(D_d^{\text{raw}} - D_d^I\right), \tag{5}$$

where the second term represents the vacancy contribution.

For the screw dislocation, the diffusivities D_d^v computed from Eq. (5) are only slightly larger than the intrinsic diffusivities (Fig. 5a), indicating that the second term in Eq. (5) is relatively small. Accordingly, the Arrhenius parameters obtained in the presence of vacancies are close to those for intrinsic diffusion (Table 2). In other words, although the introduction of a single vacancy produces a large enhancement of the core diffusivity, the recalculation to the equilibrium vacancy concentration reduces the vacancy contribution to a small correction.

Similar calculations have been performed for the edge dislocation. In this case, however, the situation is very different. At temperatures below 950 K the contribution of the intrinsic diffusivity is negligibly small and Eq. (5) can be applied in the approximate form $D_d^v = N_v D_d^{\text{raw}}$. At higher temperatures, where the rapidly increasing intrinsic diffusivity becomes large, the D_d^v values computed from Eq. (5) come close to D_d^I. At these temperatures, the edge dislocation core is capable of generating its own point defects and the addition of a vacancy does not produce any

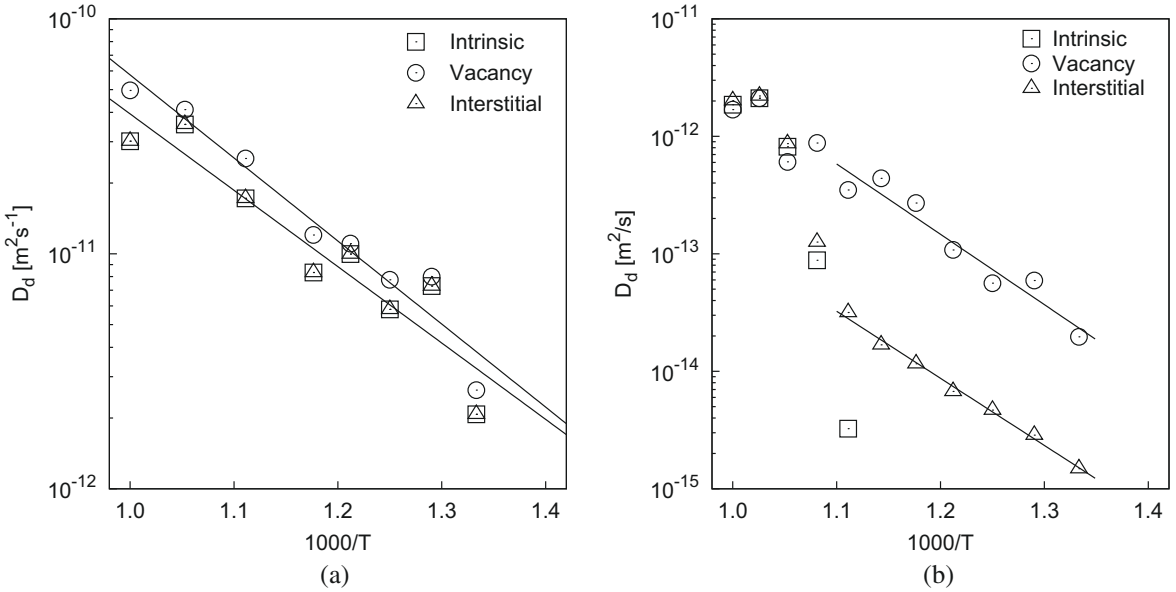

Fig. 5. Arrhenius plots of calculated diffusion coefficients in (a) the screw dislocation core and (b) the edge dislocation core. The lines show Arrhenius fits in the selected temperature intervals.

Table 2
Arrhenius parameters of diffusion along the screw and edge dislocations in Al computed in this work. The diffusion radius of the core r_d is also indicated. The error bars are represented by standard deviations.

	Intrinsic	With vacancy	With interstitial
Screw dislocation			
E_d (eV)	0.64 ± 0.10	0.70 ± 0.07	0.64 ± 0.10
$\log D_{0d}$ (m^2/s)	-7.16 ± 0.57	-6.71 ± 0.40	-7.15 ± 0.57
r_d (nm)	0.59 ± 0.001	0.61 ± 0.006	0.60 ± 0.003
Edge dislocation			
E_d (eV)	–	1.19 ± 0.14	1.13 ± 0.04
$\log D_{0d}$ (m^2/s)	–	-5.65 ± 0.89	-7.21 ± 0.24
r_d (nm)	–	1.16 ± 0.13	0.89 ± 0.03

significant effect. The diffusion coefficients calculated for the edge dislocation are shown in Fig. 5b. Considering the different roles of the added vacancy at low and high temperatures, the Arrhenius parameters (Table 2) were computed by fitting to the diffusion coefficients obtained only at temperatures below 950 K.

3.4. Interstitial diffusion in dislocation cores

Due to the high mobility of interstitials, the difference between D_d^{raw} and D_d^I is greater than in the vacancy case and at low temperatures easily reaches an order of magnitude. This fact offers an opportunity to cross-check our methodology. Indeed, since we keep only one interstitial in the simulation block at all temperatures, the Arrhenius fit to D_d^{raw} should give us an effective interstitial migration energy E_{im} in the core region. For the screw dislocation, assuming that at $T \leqslant 900$ K the intrinsic contribution to D_d^{raw} can be neglected, the Arrhenius fit gives $E_{im} = 0.14 \pm 0.04$ eV. This number compares well with the migration energy of bulk interstitials computed with this EAM potential (0.15 eV) [42] and the migration energy measured experimentally (0.1 eV) [1]. Equally encouraging results have been obtained for the edge dislocation.

The true dislocation diffusivity D_d^i in the presence of equilibrium interstitials is computed from the equation

$$D_d^i = D_d^I + N_i\left(D_d^{\text{raw}} - D_d^I\right), \tag{6}$$

where the equilibrium number N_i of interstitials that would be found in the simulation block is given by Eq. (3). For the screw dislocation, the obtained D_d^i values are almost identical to D_d^I due to the very small magnitude of N_i. Although D_d^{raw} is much larger than D_d^I, typical values of N_i are on the order of 10^{-3}–10^{-4}, making the second term in Eq. (6) negligibly small. Thus, interstitials are predicted to give practically no contribution to the diffusivity in the screw dislocation in comparison with intrinsic diffusion (Fig. 5a), leading to $E_d^i \approx E_d^I \approx 0.64 \pm 0.10$ eV (Table 2).

By contrast, in the edge dislocation the intrinsic diffusivity is so small that it can be completely neglected at all temperatures below 925 K. The Arrhenius plot of D_d^i at these temperatures (Fig. 5b) was used to extract the activation energy and pre-factor listed in Table 2. At higher temperatures, the situation changes as the rapidly increasing intrinsic diffusivity reaches and then exceeds the interstitial contribution. This temperature range is dominated by a different diffusion regime and was not included in the Arrhenius fit.

4. Discussion and conclusions

Fig. 5 and Table 2 summarize the main findings of this work. Self-diffusion coefficients have been computed for the screw and edge dislocations in Al in the presence of vacancies, interstitials and without any pre-existing defects

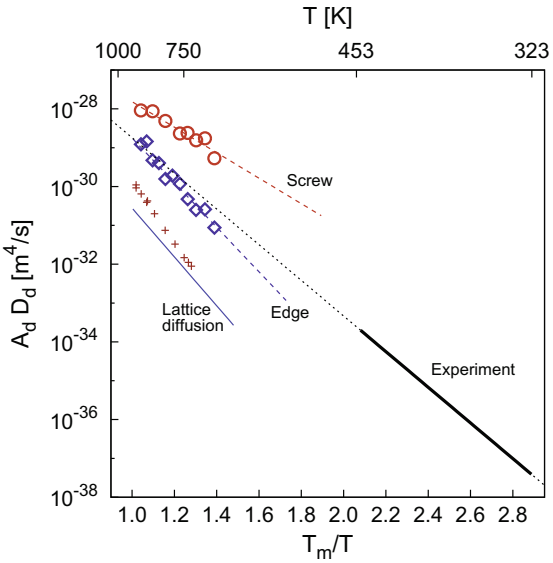

Fig. 6. Arrhenius diagrams of the calculated diffusion flux $P_d = A_d D_d$ for the screw (◯) and edge (◇) dislocations in comparison with experimental data [24] measured at temperatures 323–453 K (thick solid line). The dashed and dotted lines show Arrhenius fits. Experimental (+) [51] and computed (thin solid line) data for lattice self-diffusion is shown for comparison.

(intrinsic diffusion) over a range of temperatures. We find that diffusion along the screw dislocation is dominated by the intrinsic mechanism, with vacancies and interstitials making only minor contributions. In contrast, intrinsic diffusion in the edge dislocation is very slow at all temperatures below 950 K, and the core diffusivity is dominated by vacancies. At high temperatures (>950 K), the core of the edge dislocation becomes increasingly disordered and begins to operate as an effective source of point defects. As a result, the core diffusivity remains high even when no point defects are introduced prior to the MD simulations, and when such defects are introduced, they produce little effect on the core diffusivity. Overall, diffusion along the screw dislocation is found to be significantly faster than diffusion along the edge dislocation. These results demonstrate that diffusion rates and diffusion mechanisms strongly depend on the dislocation type.

The diffusion radius of the dislocation core is about 0.6 nm of the screw dislocation and about 1 nm for the edge dislocation. Both numbers are physically reasonable and validate the assumption $r_d = 0.5$ nm commonly accepted in the continuum models of dislocation diffusion [3]. No temperature dependence of r_d was detected within the error bars of the simulations.

The only experimental data that can be used for comparison with our simulations was obtained by indirect measurements based on void-shrinkage kinetics in thin films [24]. Such measurements give only the integrated flux $P_d = D_d A_d$, A_d being the cross-sectional area of the core. To enable comparison with this experiment, we have computed the integrated flux by adding the contributions of different mechanisms,

Table 3
Arrhenius parameters of dislocation diffusion obtained from Fig. 6.

	Screw	Edge	Experiment
E_d (eV)	0.68 ± 0.08	1.19 ± 0.14	0.85
$\log P_{0d}$ (m^4/s)	-24.54 ± 0.47	-23.01 ± 0.85	−24.15
E_d/E	0.58	0.82	0.64

$$P_d = D_d^v A_d^v + D_d^i A_d^i + D_d^I A_d^I. \quad (7)$$

Because our EAM potential overestimates the experimental melting point, homologous temperatures T/T_m are used as a common basis for comparison. The computed and experimental fluxes are plotted on the Arrhenius diagram in Fig. 6. Since these two sets of data were obtained in very different temperature intervals, extrapolation across a wide range of temperatures is made. Nevertheless, we observe that the experimental Arrhenius line extrapolates to the same range of P_d values at high temperatures as obtained by our simulations. Furthermore, the experimental measurements represent an average diffusivity over different types of dislocations present in the experimental samples. It is, therefore, encouraging to see that the extrapolated experimental values of P_d lie between our calculations for the limiting cases of the screw and edge dislocations. Considering all the uncertainties involved in this comparison, the agreement between the experiment [24] and simulation is quite satisfactory.

Table 3 summarizes the effective Arrhenius parameters for the screw and edge dislocations obtained by fitting to the fluxes P_d. As expected from Fig. 6, the experimental activation energy for an "average" dislocation lies between the computed activation energies for the screw and edge dislocations. Furthermore, the computed ratios of the dislocation to lattice activation energies are, respectively, on the lower and higher sides of the experimental range 0.6–0.7 [1]. Our finding that the Arrhenius characteristics of dislocation diffusion depend on the dislocation type is also in agreement with experimental data [1–3].

To put the obtained dislocation diffusivities in perspective, Fig. 6 includes data for lattice self-diffusion. The lattice self-diffusion coefficients were calculated by standard methods [50,35] based on the transition state theory, with the vacancy formation and migration energies computed by molecular statics (Table 4).[1] To enable plotting in the same coordinates, the computed and experimental diffusion coefficients were multiplied by πr_d^2 with $r_d = 0.5$ nm. The most reliable experimental data is represented by direct radiotracer measurements by Lundy and Murdock [51]. Two conclusions can be drawn from this comparison. First, the reasonable agreement between the calculated and experimental lattice diffusivities is a reassurance of accuracy of our methodology. Second, this comparison

[1] This calculation of the lattice diffusivity is correct only in the limit of low temperatures and can give errors when extrapolated to high temperatures. This approximation is used here only for the purpose of putting the dislocation diffusivities in perspective with lattice diffusion.

Table 4
Calculated vacancy formation energy (E_{vf}), formation entropy (S_{vf}), migration energy (E_{vm}), attempt frequency (ν) and lattice constant (a) used for the calculation of the lattice self-diffusion coefficient in Al.

E_{vf} (eV)	S_{vf}/k_B	E_{vm} (eV)	ν (Hz)	a (Å)
0.675	−0.360	0.630	6.00×10^{12}	4.05

confirms that dislocation diffusion remains faster than lattice diffusion even at temperatures approaching the melting point. At 0.5 T_m, the difference between the two types of diffusivity reaches 2–3 orders of magnitude.

We now discuss atomic mechanisms of dislocation diffusion. Two mechanisms have been identified in this work as most important: the intrinsic diffusion and the vacancy-mediated diffusion. The role of interstitials is relatively small; although their mobility is very high, the formation energy is too large resulting in extremely small concentrations and thus insignificant contributions to diffusion.

The intrinsic diffusion mechanism is a rather intriguing phenomenon that does not occur in lattice diffusion under normal conditions. Although we have not been able to achieve a full understanding of the underlying atomic mechanism, the following observations might give some clue.

First, the intrinsic simulations at temperatures above 800 K reveal rare events in which a vacancy is injected from the core into nearby lattice regions. The vacancy makes several jumps in the lattice and quickly returns to the core. Evidence of such events is obtained by plotting atomic trajectories between sequential MD snapshots, as shown in Fig. 7a for the screw dislocation at 850 K. A chain of arrows connecting lattice sites shows a trace of a vacancy walk through those sites. A snapshot containing an injected vacancy that is still in the lattice would contain a chain of arrows originating from a lattice site (which would indicate the current vacancy position) and ending in the core. A set of arrows forming a loop starting and ending in the core indicates a vacancy excursion into the lattice and back into the core. Such loops were indeed frequently observed at high temperatures, with the exit point of the vacancy being generally different from the reentry point into the core. At all temperatures below 950 K, none of our snapshots contained a vacancy in the lattice, suggesting that the vacancy excursions were much shorter than 0.2 ns. Note that when a vacancy is injected into the lattice, an interstitial is left in the core, which is free to migrate along the core until the vacancy returns and recombines with it.

Based on these observations we suggest the following mechanism of intrinsic diffusion. Once in a while, a Frenkel defect (vacancy–interstitial pair) spontaneously forms in the core by thermal fluctuations. The two defects briefly separate and migrate along the core independently, producing self-diffusion before they recombine and restore the defect-free structure. Because the interstitial formation energy in the lattice is very high, it always stays in the core during this process. The vacancy, on the other hand, has a finite probability of making a few jumps into adjacent lattice regions and returning into the core, giving rise to chains of atomic displacements seen in our simulations. Thus, the intrinsic diffusion can be attributed to the existence of dynamic Frenkel pairs in the dislocation core.

The second clue is that the screw dislocation core is seen to form dynamic jogs at relatively high temperatures (Fig. 8). The jogs typically nucleate by pairs, spread along the core and recombine with their periodic images. As a result, the dislocation line fluctuates around an average position. By contrast, no thermal jogs or kinks were found at the edge dislocation in our simulations. Given that the intrinsic diffusion is dominant in the screw core and negligibly small in the edge core, we hypothesize that the thermal jogs *might* be involved in the Frenkel pair formation. It seems possible that the jogs create local atomic configurations

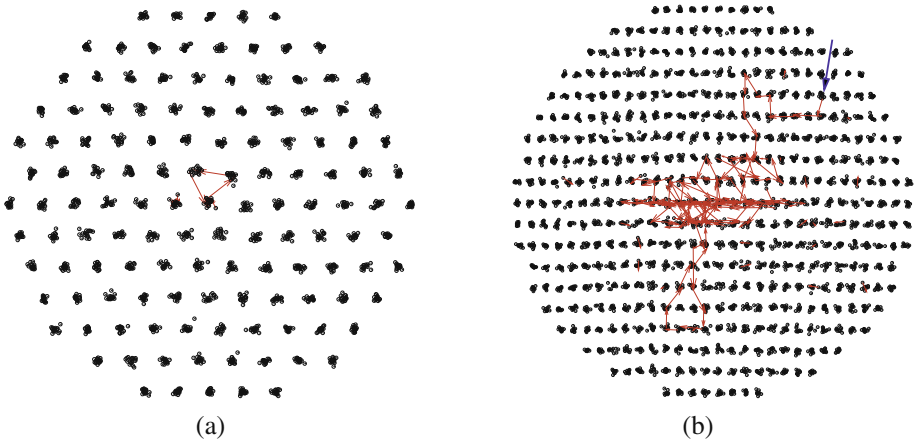

Fig. 7. Typical cross-sectional views of the simulation block showing vacancy migration paths without any pre-existing point defects in the dislocation core (intrinsic case). (a) Screw dislocation at 850 K. (b) Edge dislocation at 1000 K. The dislocation line is normal to the page. The small black circles show projections of dynamic atoms. The red arrows indicate atomic displacements between two snapshots separated by 0.2 ns. The blue arrow show the location of a vacancy generated by the dislocation core. (For interpretation of the references to colour in this figure legend, the reader is referred to the web version of this article.)

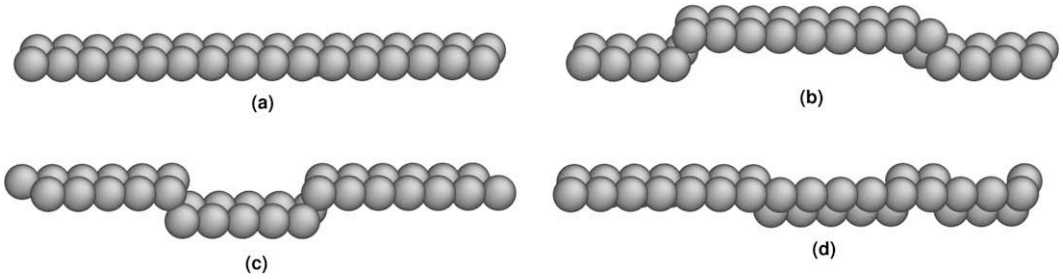

Fig. 8. Typical configurations of the screw dislocation core at 750 K without any pre-existing point defects, showing the formation of thermal jogs. (a) Straight dislocation; (b and c) double jogs with screw segments in parallel glide planes; (d) multiple jogs with some of the screw segments in intersecting glide planes. The edge segments are usually as short as one Burgers vector. The core structure is visualized using the centrosymmetry parameter [63].

that facilitate Frenkel pair nucleation, but this connection between the two processes would need to be tested in future studies. In this work we tried but have not been able to confirm a correlation between the jog formation and vacancy excursions around the core.

At temperatures 950 K and above, the intrinsic diffusion mechanism changes. We begin to see vacancies frequently abandoning the core and performing relatively long walks (0.6 ns or longer) in the surrounding lattice. Such vacancies are readily revealed by arrow plots, as demonstrated in Fig. 7b for the edge dislocation. Some of the snapshots contained more than one vacancy path and/or more than one vacancy present in the lattice simultaneously. Together with significant structural distortions observed in the core region, these findings suggest that the core apparently becomes an effective supplier of point defects.

Finally, when a single vacancy is introduced into the core prior to the MD simulations, the arrow plots reveal its occasional excursions into the lattice. Their frequency is larger and the duration much longer than in the intrinsic case, and both increase with temperature. However, only one vacancy is always present in the simulation block. It is only at high temperatures approaching T_m that the core acquires the ability to generate additional vacancies, which is illustrated in Fig. 7b.

An interesting topic of future research would be to compare these results with dislocation diffusion in a low stacking fault energy metal such as copper. If the existence of the intrinsic diffusivity is confirmed as a generic effect, it might motivate a revision of the current understanding of the role of point defects in atomic transport along dislocations. Furthermore, this would warrant a re-examination of the models of materials processes that rely on the assumption of vacancy-mediated diffusion, particularly models that invoke changes in dislocation diffusion as a result of vacancy over- or under-saturation in the material.

Acknowledgement

This work was supported by the US Air Force Office of Scientific Research, Structural Mechanics Program.

References

[1] Balluffi RW, Granato AV. In: Nabarro FRN, editor. Dislocations in solids, vol. 4. Amsterdam: Elsevier/North-Holland; 1979. p. 1–133.
[2] Sutton AP, Balluffi RW. Interfaces in crystalline materials. Oxford: Clarendon Press; 1995.
[3] Kaur I, Mishin Y, Gust W. Fundamentals of grain and interphase boundary diffusion. Chichester (West Sussex): Wiley; 1995.
[4] Pun GPP, Mishin Y. Defect Diffus Forum 2007;266:49.
[5] Monzen R, Asaoka J, Kita K, Kitagawa K. J Jpn Inst Metals 1998;62:363.
[6] Lesuer DR, Syn CK, Whittenberger JD, Carsi M, Ruano OA, Sherby OD. Mater Sci Eng A 2001;317:101.
[7] Satyanarayana DVV, Malakodaiah G, Sarma DS. Mater Sci Eng A 2002;323:119.
[8] Cottrell A, Bilby BA. Proc Phys Soc Lond 1949;62:49.
[9] Schwink C, Nortmann A. Mater Sci Eng A 1997;234:1.
[10] Xu Z, Picu RC. Modelling Simulat Mater Sci Eng 2006;14:195.
[11] Varschavsky A, Donoso E. Mater Lett 1997;31:239.
[12] Le Gall RE, Saindrenan G. Interface Sci 2003;11:59.
[13] Kempshall BW, Prenitzer BI, Giannuzzi LA. Scripta Mater 2002;47:447.
[14] Kolbe M, Dlouhy A, Eggeler G. Mater Sci Eng A 1998;246:133.
[15] Sundaresan R, Raghuram AC, Mallaya RM, Vasu KI. Powder Metall 1996;39:138.
[16] Estrin Y, Rabkin E. Scripta Mater 1998;39:1731.
[17] Amador DR, Monge MA, Torralba JM, Pareja R. Appl Phys A 2005;80:803.
[18] Baker SP, Joo YC, Knaub MP, Arzt E. Acta Mater 2000;48:2199.
[19] Shima Y, Ishikawa Y, Nitta H, Yamazaki Y, Mimura K, Isshiki M, et al. Mater Trans 2002;43:173.
[20] Sakaguchi I, Yurimoto H, Sueno S. Solid State Commun 1992;84:889.
[21] Nakagawa T, Nakamura A, Sakaguchi I, Shibata N, Peter K, Lagerlöf D, et al. J Ceram Soc Jpn 2006;114:1013.
[22] Wang ZM, Shiflet GJ. Metall Mater Trans A 1998;29:2073.
[23] Tang X, Peter K, Lagerlöf D, Heuer AH. J Am Ceram Soc 2003;86:560.
[24] Volin TE, Lie KH, Balluffi RW. Acta Metall 1971;19:263.
[25] Tan Q, Ke TS. Phys Status Solidi A 1990;122:K25.
[26] Miller KM, Ingle KW, Crocker AG. Acta Metall 1981;29:1599.
[27] Huang J, Meyer M, Pontikis V. Phys Rev Lett 1989;63:628.
[28] Huang J, Meyer M, Pontikis V. Philos Mag A 1991;63:1149.
[29] Boehm J, Nieminen RM. Phys Rev B 1994;50:6450.
[30] Hoagland RG, Voter AF, Foiles SM. Scripta Mater 1998;39:589.
[31] Fang QF, Wang R. Phys Rev B 2000;62:9317.
[32] Grabowski S, Kadau K, Entel P. Phase Transit 2002;75:265.
[33] Picu RC, Zhang D. Acta Mater 2004;52:161.
[34] Jannot E, Mohles V, Gottstein G, Thijsse B. Defect Diffus Forum 2006;249:47.

[35] Mishin Y. In: Gupta D, editor. Diffusion processes in advanced technological materials. Norwich (NY): Noyes Publications/William Andrew Publishing; 2005. p. 113–71.
[36] Sørensen MR, Mishin Y, Voter AF. Phys Rev B 2000;62:3658.
[37] Mishin Y, Gust W. Ionics 2001;7:247.
[38] Suzuki A, Mishin Y. Interface Sci 2003;11:131.
[39] Suzuki A, Mishin Y. Interface Sci 2003;11:425.
[40] Suzuki A, Mishin Y. J Metastable Nonocryst Mater 2004;19:1.
[41] Suzuki A, Mishin Y. J Mater Sci 2005;40:3155.
[42] Mishin Y, Farkas D, Mehl MJ, Papaconstantopoulos DA. Phys Rev B 1999;59:3393.
[43] Ivanov VA, Mishin Y. Phys Rev B 2008;78:064106.
[44] Schaefer HE, Gugelmeier R, Schmolz M, Seeger A. Mater Sci Forum 1987;15–18:111.
[45] Balluffi RW. J Nucl Mater 1978;69–70:240.
[46] Stroh AN. Philos Mag 1958;3:625.
[47] Hartley CS, Mishin Y. Acta Mater 2005;53:1313.
[48] Woodward C, Trinkle DR, Hector LG, Olmsted DL. Phys Rev Lett 2008;100:045507.
[49] Stadler J, Mikulla R, Trebin HR. Int J Mod Phys C 1997;8:1131.
[50] Philibert J. Atom movements – diffusion and mass transport in solids. Les Ulis: Les Editions de Physique 1991.
[51] Lundy TS, Murdock JF. J Appl Phys 1962;33(May):1671.
[52] Engardt RD, Barnes RG. Phys Rev B 1971;3(April):2391.
[53] Spokas JJ, Slichter CP. Phys Rev 1959;113(March 15):1462.
[54] DeSorbo W, Turnbull D. Phys Rev 1959;115(August 1):560.
[55] Fradin FY, Rowland TJ. Appl Phys Lett 1967;11(September):207.
[56] Stoebe TG, Dawson HI. Phys Rev 1968;166(February):166.
[57] Häßner A. Kristall u Technik 1974;9:1371.
[58] Gangulee A, d́Heurle FM. Thin Solid Films 1975;25:317.
[59] Levenson LL. Appl Phys Lett 1989;55(December):2617.
[60] Haruyama O, Kawamoto H, Yamaguchi H, Yoshida S. Jpn J Appl Phys 1980;19:807.
[61] Federighi T. Philos Mag 1959;4:502.
[62] Volin TE, Balluffi RW. Phys Status Solidi 1968;25:163.
[63] Kelchner CL, Plimpton SJ, Hamilton JC. Phys Rev B 1998;58:11085.